

Acoustic resonance testing of additive manufactured lattice structures

Y. Ibrahim¹, Z. Li², C. M. Davies¹, C. Maharaj³, J. P. Dear¹, P. A. Hooper¹

¹Department of Mechanical Engineering, Imperial College London, London, SW7 2AZ, UK

² AVIC Manufacturing Technology Institute, Beijing, 100024, P.R. China

³ Department of Mechanical and Manufacturing Engineering, The University of the West Indies, St. Augustine, Trinidad and Tobago

ABSTRACT

Additive manufacturing (AM) allows engineers to design and manufacture complex weight saving lattice structures with relative ease. These structures, however, present a challenge for inspection. A non-destructive testing and evaluation method used to assess material properties and quality is the focus of this paper, namely acoustic resonance (AR) testing. For this research, AR testing was conducted on weight saving lattice structures (fine and coarse) manufactured by powder bed fusion. The suitability of AR testing was assessed through a combined approach of experimental testing and FE modelling. A sensitivity study was conducted on the FE model to quantify the influence of element coarseness on the resonant frequency prediction and this needs to be taken into account in the application and analysis of the technique. The analysis was extended to extract effective modulus values for the lattice structures and the solid materials from every detected overtone, allowing for multiple measurements from a single AR test without the need to carefully isolate the fundamental. The AR and FE modelling modulus of elasticity values were validated using specimens of known properties. There was fair agreement between the FE and compression test extracted values of effective modulus for the coarse lattice. For the fine lattice, there was agreement in the values of effective modulus extracted from AR, 3-point bend, and compression experimental tests carried out. It was found that loose powder fusing from AM resulted in the fine lattice structure having a higher density (at least 1.5 times greater) than calculated due to the effect of loose powder adhesion. This effect resulted in an increased stiffness of the fine lattice structure. AR can be used as a measure of determining loose powder adhesion and other unique structural characteristics resulting from AM.

KEY WORDS: Additive manufacturing; Powder bed fusion; Selective laser melting; Lattice structures; acoustic resonance; 316L stainless steel

1 INTRODUCTION

Industrial manufacturing demands stringent quality control and a comprehensive understanding of the influence of the manufacturing process on the material properties. Additive manufacturing (AM) processes are fast evolving from their rapid-prototyping past to become manufacturing processes that are viable for industrial application [1]. To assist this transition, complementary non-destructive evaluation methods are needed to inspect parts, especially where designs contain complex geometries.

Lattice structures are a good example of the design flexibility offered by AM. These structures consist of cellular repeating elements, which often lead to very complex internal geometries. This complexity is a major

obstacle when attempting to manufacture these structures with conventional manufacturing methods, which often rely on methods that relinquish control over the micro-architecture [2]. Lattice structures with complex architecture can be applied to a wide range of fields where very efficient material usage is beneficial. Computer-aided design may also be used to design lattice structures with specified mechanical properties that can greatly differ from that of the parent material [3], [4].

Xiao et al. [5] investigated Face Centre Cube (FCC), Vertex Cube (VC), and Edge Centre Cube (ECC) lattice structures and found that the FCC and VC lattice structures had improved mechanical behaviour compared with that of the ECC lattice structure. However the ECC lattice structure had energy absorption efficiency. For triangular lattice structures, Niu et al. [6] found that the beam thickness had the most significant effect on the effective tensile elastic modulus. Using morphological analysis and image-based simulations of design files, du Plessis et al. [7] determined that strut-based lattices and minimal surface designs are suitable for bone implants. An optimal design can be tailored to the specific performance requirements. Compared to the commonly used longitudinal fin solid heat sinks, Shamvedi et al. [8] found that lattice structure heat sinks of varying sizes underperformed under natural convection.

The characterisation of the material properties of lattice structures can be challenging, especially with the influence of the AM process, specifically direct metal laser sintering. For a Titanium-tantalum lattice structure, Sing et al. [9] found that the elastic constant and yield strength were very sensitive to laser power. An increase in laser power or laser scan speed was found to decrease the effects of loose powder adhesion on the struts of the lattice structures [10]. For 316 stainless steel powder, Fatemi et al. [11] observed that an increase in current and frequency led to an increase in the thickness and density of samples. Also, an increase in scan speed decreased the layer thickness and density of samples. Some conventional characterisation tests, such as quasi-static uniaxial compression, may be applied directly to the structures while other tests require some degree of adaptation.

The current generation of AM machines give a large variation in the material properties from one part to the next, introducing great difficulty in determining the quality of each manufactured component [12], [13]. This stems from limited process control due to multiple factors that affect the manufacturing process such as the raw material properties and part geometry. This problem necessitates quick and non-destructive evaluation methods to rapidly assess the quality of the manufactured components on site.

Acoustic resonance (AR) testing is an attractive non-destructive evaluation method in the context of industrial manufacturing, where a component is dynamically excited and its vibrational resonance frequency measured. Every part has a unique resonant signature that is related to its material properties. Material properties such as the effective elastic modulus and Poisson's ratio can be quickly calculated from this measurement [14]. This type of testing is well established for solid components (ASTM E1876) [14], and less so for lattice structures. AR has been used as an inspection tool to determine parts with voids, cracks, out-of-tolerance dimensions, bonding issues, and missed manufacturing processes. A deviation from the expected resonant signature can indicate the presence of a structural flaw or variation.

This paper investigates the applicability of this class of testing to AM lattice structures. Bulk and lattice samples were manufactured and subject to AR testing as well a quasi-static testing to obtain independently

measurements for the effective elastic modulus by. A dynamic finite element (FE) model was developed to simulate the test and assess the ability of the model to estimate correctly the resonant frequencies expected. Some adaptive measures are then suggested to increase the reliability of these tests specifically for AM lattice structures.

2 METHODS

2.1 Lattice structure sample design

The lattice structure chosen for this study was based on the well-known regular hexagon honeycomb tessellation extended into a three-dimensional representation. The repeating unit cell and resulting structure is shown in Figure 1. The geometric parameters shown in Figure 1 determine the shape of the unit cell and therefore the geometry of the resulting lattice. Setting $a=b=L$ and angles α and β to 30° generate the traditional hexagonal honeycomb. This was kept consistent throughout this study.

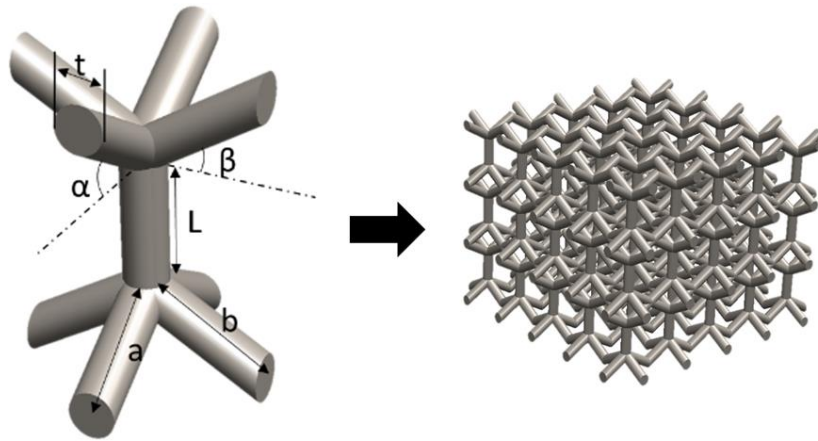


Figure 1: The repeating double-honeycomb unit cell and the resulting lattice structure. The geometric parameters shown on the unit cell may be varied to produce different unit cell geometries.

It is important to note that in keeping the cellular geometry the same, this keeps the relative density the same. This is the density of the whole lattice structure compared to that of the parent material. It has been shown by Ashby et al. [3] that the mechanical properties of the lattice structure depend significantly on the relative density [3], [4]. This was kept constant throughout the study for this reason. A nominal design value for relative density of 12% was selected, which corresponds to the resulting relative density achieved by setting the parameters shown in Figure 1 to the values shown in Table 1. The cellular geometry was simply scaled down in the case of the AR tests in order to generate reasonably sized samples that fit within the build volume of the machine used for manufacturing. The effective modulus, E_{eff} , of the lattice structures is defined as the Young's modulus, E , of an equivalent homogeneous material with the same stiffness properties as the lattice structure [4].

Table 1: The values used for the dimensional parameters of the unit cell of the compression test samples and the AR test samples.

Parameter	Dimension	
	Compression Test	AR Test†

	Coarse lattice	Fine lattice	Fine lattice
a (mm)	1.25	0.75	0.75
b (mm)	1.25	0.75	0.75
L (mm)	1.25	0.75	0.75
t (mm)	0.40	0.24	0.24
α (°)	30	30	30
β (°)	30	30	30
Cell envelope (mm)	2.17 x 2.17 x 2.5	1.30 x 1.30 x 1.5	1.30 x 1.30 x 1.5

† It was not possible to build a coarse lattice AR test sample due to manufacturing constraints. The AR sample cell size was reduced in order to allow the entire specimen to fit within the build volume whilst maintaining the correct sample aspect ratio required for the AR test.

2.2 Sample manufacturing

Powder bed fusion (PBF) was the process used to build the experimental samples tested in this investigation. Gas atomised 316L stainless steel powder with a particle size range of 10-45 μm was used. The samples, shown in Figure 2, were manufactured using the Concept Laser M lab Cusing R machine [15]. The layer thickness was set to 25 microns and the laser scan speed was set to 1000 mm/s with a laser power of 100 W.

These laser parameters chosen were based on previous studies conducted [16-17] and found to produce the most faithful representation of the intended geometry particularly in the context of lattice structures with circular beams. Fully solid AR samples were also manufactured using the same AM machine for further assessment of the properties of the as-built material (refer to Figure 3).

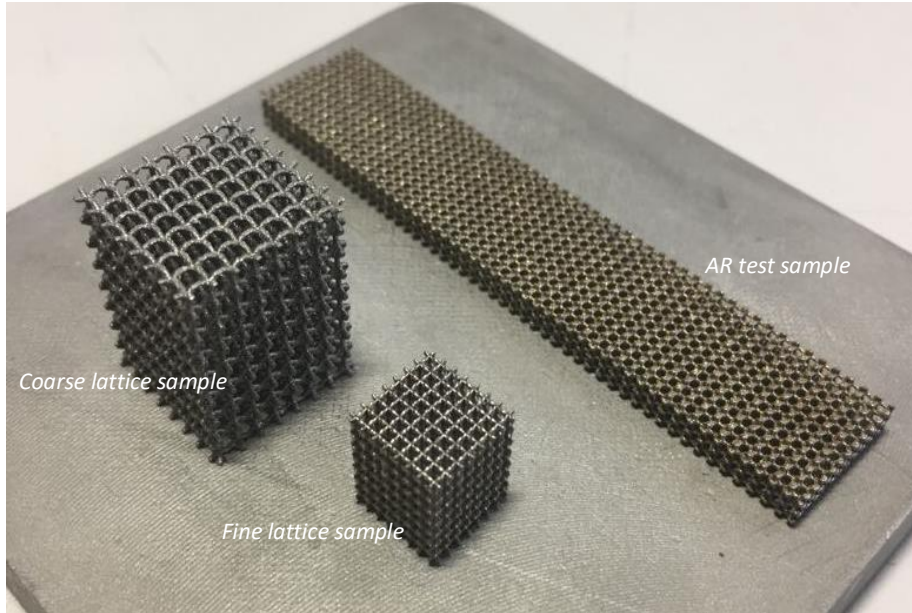


Figure 2: The AM lattice structure samples

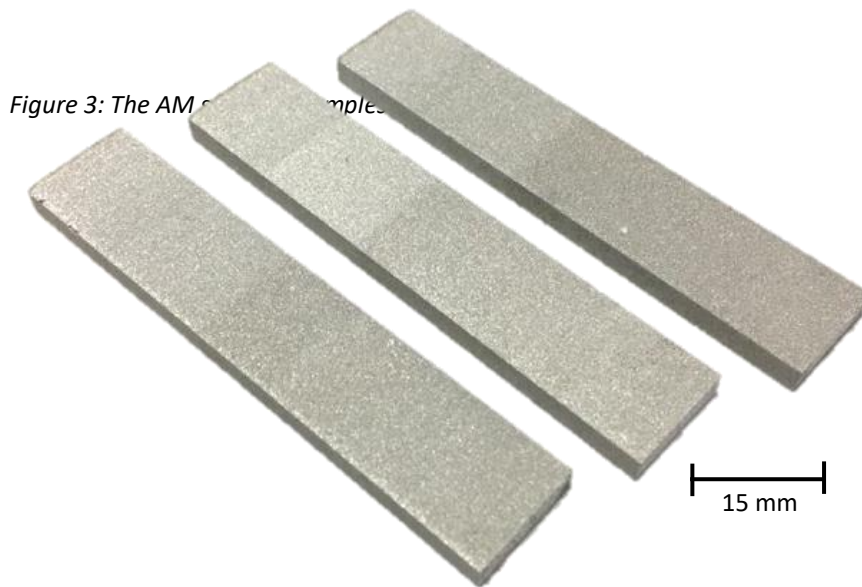


Figure 3: The AM samples

2.3 Relative density measurement

The relative density of the lattice structures was measured to evaluate the quality of the additive manufactured samples. The mass of the samples was measured in air and the total volume was measured directly using digital callipers, treating the lattice structure as a homogenous solid bar.

2.4 Quasi-static compression and 3-point bend testing

Compression samples filled with the coarse and fine lattice architecture shown in Figure 1 were subject to uniaxial quasi-static compression testing in order to measure the effective modulus of the non-deformed lattice structure. This was achieved through intermittent loading and unloading of the lattice structure sample, with the measurement taken from the unloading curve. This is suggested by Ashby et al. [18] to minimise the effect of any malformations in the lattice on the measurements due to manufacturing defects. The structure is first loaded to 75% of its yield strength followed by complete unloading. The extraction of compressive properties was done under the guidance of ASTM D 1621-16 [19].

Standard three-point bend tests were performed on the same lattice structure samples manufactured using AM to provide additional means of measuring the effective modulus of the samples using deformation similar to that which occurs during the AR tests. The free-free vibration modes of interest occur mainly as flexural deformation. The extraction of flexural properties was done under guidance of ASTM D790—17 [20], which was adapted to facilitate the testing of metal lattice structures in this study.

2.5 AR testing

Ten AR test samples consisting of the lattice described in Figure 1 as well as fully solid rectangular samples were constructed using AM in accordance with the design rules outlined in the ASTM E1876 test standard for the resonance testing of solid metallic materials [14]. Wrought 316L stainless steel samples as well as 6082 T6 aluminium alloy samples, with known elastic moduli, were also prepared (Table 2) to calibrate and verify the test setup and the signal processing method used. Simple rectangular cross-section bar-type samples were used with carefully selected width to length and thickness to length ratios in order to ensure the resonant frequency of the samples lies within the audible acoustic range [14]. This also allows for simplifications to be made in the calculations used to determine the dynamic properties.

Table 2: The AR test sample specifications.

Sample	Length, L (mm)	Width, W (mm)	Thickness, T (mm)	Mass, m (g)
6082 – T6 Aluminium	99.9 ± 0.1	14.7 ± 0.1	3.8 ± 0.1	14.6 ± 0.1
Wrought 316L Stainless Steel	149.9 ± 0.1	25.1 ± 0.1	3.0 ± 0.1	86.2 ± 0.1
AM Solid 316L Stainless Steel	77.6 ± 0.1	15.6 ± 0.1	4.1 ± 0.1	36.6 ± 0.1
AM Lattice 316L Stainless steel	77.2 ± 0.1	15.5 ± 0.1	3.9 ± 0.1	7.4 ± 0.05

The samples were supported on foam knife-edges positioned at each node of the fundamental resonant frequency. This is achieved through positioning the supports at 0.254 L from either edge, where L is the sample length. The sample is then excited with a small impact at the centre anti-node, with the transducer pick up (microphone) at either edge anti-node. These precautions favour the excitation of the fundamental frequency and minimise the involvement of the higher overtones in the measurement. However, the overtones will always be present to some extent and can be used to extract additional elastic modulus values as also shown in this

paper. The impact is administered using a small impactor consisting of a light weight polymer handle with a 5mm hardened steel ball attached to one end.

Figure 4 shows a schematic of the test set-up as well as the solid calibration samples and the lattice structure samples. The lattice structures are orientated such that the fundamental resonant vibrational mode imposes strain along the build direction of the lattice. This is to minimise anisotropy effects present in the structure and also means that the measured values of modulus from AR are comparable with those derived from the quasi-static compression testing.

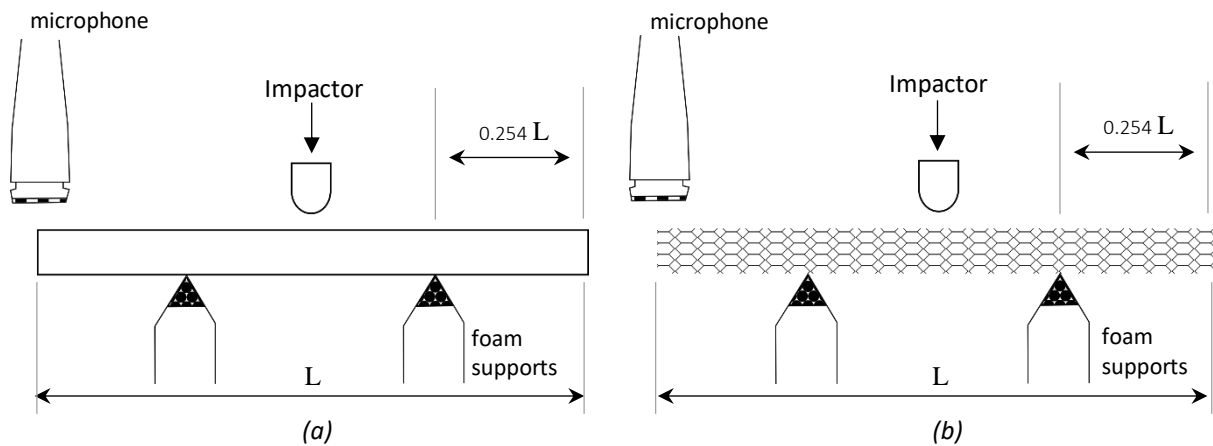


Figure 4: Schematic of the set up used to measure the resonant frequency of: a) solid rectangular bar samples and b) AM lattice samples.

The audio signal from the transducer is amplified and imported into MATLAB, where it is fed through a Fast-Fourier transfer (FFT) function to plot the frequency spectrum and identify the fundamental resonant frequency. A script was written to carry out the FFT and identify the fundamental frequencies while filtering out any environmental noise as well as any electrical noise originating from the power supply. The sampling rate used for the recorded audio is 44.1 kHz, using samples of length 10,000 points. The detectable frequency range is consequently 5 – 22,000 Hz.

In addition, the lattice structure resonance tests were performed again using high speed photography to verify the vibrational modes measured and ensure no torsional or longitudinal modes were being heavily excited. A frame rate of 16,000 frames per second was employed.

2.6 Resonance test extension using overtones

The standard resonance test was extended to obtain the material property measurements from each detected overtone in addition to the fundamental frequency. This allows the extraction of multiple measurements from a single test. It is necessary in this case however to identify the correct order of each measured frequency. Equation 2.1 denotes the relationship between the natural frequencies of a free-free beam and the material properties of the constituent material of the beam:

$$\omega_n = \sqrt{\frac{EI}{\rho A}} k^4 \quad [2.1]$$

where the Young's modulus, E , the second moment of area, I , the density, ρ , the cross-sectional area, A , and the wavenumber, k , determines the order of the natural frequency as given by Equation 2.2:

$$\cosh(kL) \cos(kL) = 1 \quad [2.2]$$

where the spatial component of the wave equation of a beam of length, L , is defined in

Figure 4. Solving Equation 2.2 for every integer rotation, n , the product of the wavenumber the beam length can be found for every order of vibration. Table 3 shows the results for the first six natural frequencies of a free-free beam from $n=0$ to $n=5$.

Rearranging Equation 2.1 and adding the $k_n L$ terms in Equation 2.3:

$$E = \frac{12 m \omega_n^2 L^3}{W T^3 (k_n L)^4} \quad [2.3]$$

where the dimensional terms W , T and L represent the width, thickness and length respectively of the cuboidal samples used for the resonance test. Note that $E = E_s$ for the solid samples and $E = E_{eff}$ for the lattice structure samples. The application of Equation 2.3 is investigated and its relevance to AM lattice structures is determined.

Table 3: Multiple solutions for kL corresponding to various orders of overtones n

N	0	1	2	3	4	5
$k_n L$	0.000	4.730	7.853	10.996	14.137	17.279

2.7 FE modelling

Dynamic response FE models were developed using the ABAQUS software package [21] in order to predict the behaviour of the lattice structures in free-free vibration and quasi-static compression. The dependence of the predicated frequencies on the material properties as well as the structural geometry was investigated. The wrought solid specimens were also modelled for independent verification of the FE method. A sensitivity study was then conducted to determine the influence of the FE lattice and element properties on the resulting values.

Quadratic beam elements were used to represent the lattice specimens. This was found to be more computationally efficient, compared to using volumetric cubic elements. Cubic elements however sufficed to represent the solid specimens due to the simpler topology. The material models used were directly informed from the measurements taken during the quasi-static compression tests as well as the density measurements taken of the samples.

A linear perturbation was used to excite the specimens under free-free constraints and the resulting fundamental frequencies were recorded, as well as the overtones. The FE model (Figure 5) was also used to determine the vibrational mode characteristic at each natural frequency in order to help determine the fundamental as well as the order of each overtone. This assists in identifying which frequencies are associated with unwanted modes, such as the longitudinal and torsional modes, which are not of interest for determining the material properties and therefore may be neglected. A sensitivity study was conducted as well to investigate the reliance of the frequencies predicted by the FE model on the coarseness of the element lattice used.

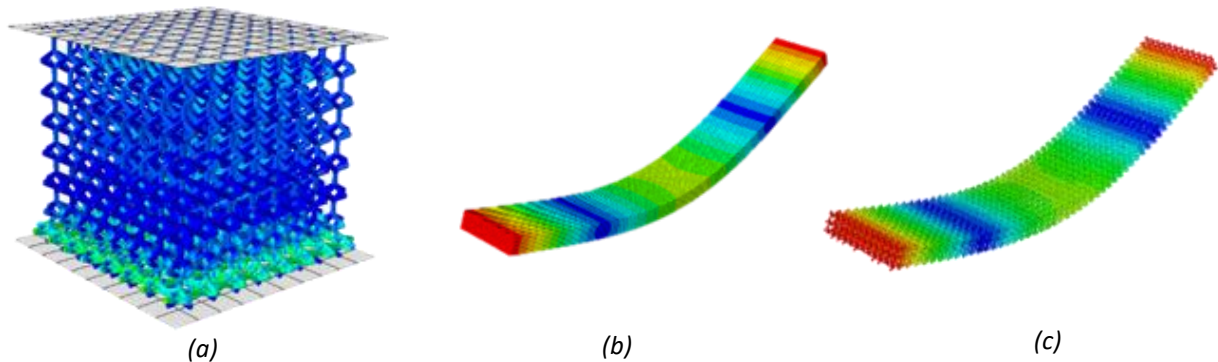


Figure 5: The FE model geometries showing: a) the lattice structure compression test, b) The solid sample AR test and c) the Lattice structure AR test. The models shown in b) and c) are excited into the fundamental mode.

3 RESULTS

3.1 Relative Density

The relative density of the lattice structures is first measured to assess the quality of the build. Table 4 tabulates the relative density measurements of the lattice structures used for the quasi-static tests and the AR tests. A dependence of the relative density on the scale of cellular geometry is evident where the smaller cell size yielded a higher relative density. The micrographs shown in Figure 6 shows a single hexagonal unit cell as found in the quasi-static compression test samples and the AR test samples. Loosely bonded powder can be seen on the surface of both structures, however it is present to a greater extent on the smaller cells of the AR test samples. The loosely bonded powder adds more mass to the fine lattice structure within the sample effective volume, thus increasing the relative density.

The fully solid samples, built in the same AM machine used to build the lattice samples, exhibit a slightly reduced relative density than expected. This is indicative of internal porosity present in the samples, arising due to incomplete fusion of the raw powder material [22], [12]. The extent of the porosity can be seen in Figure 7 showing the fracture surface of a fully solid AM sample following a three-point bend test. The laser path can be roughly seen where full fusion occurred, suggesting that porosity is more likely to occur in areas where the laser never directly passes [22].

Table 4: Test samples and their measured relative densities.

Sample	Lattice size	Relative Density (%)	Nominal design value (%)	Deviation from design value (%)
Compression Test	Coarse	13.4 ± 0.2	12	+12

Compression Test	Fine	20.6 ± 0.2	12	+72
AR Test	Fine	19.6 ± 0.2	12	+63
Fully Solid	-	92.5 ± 0.2	100	-8

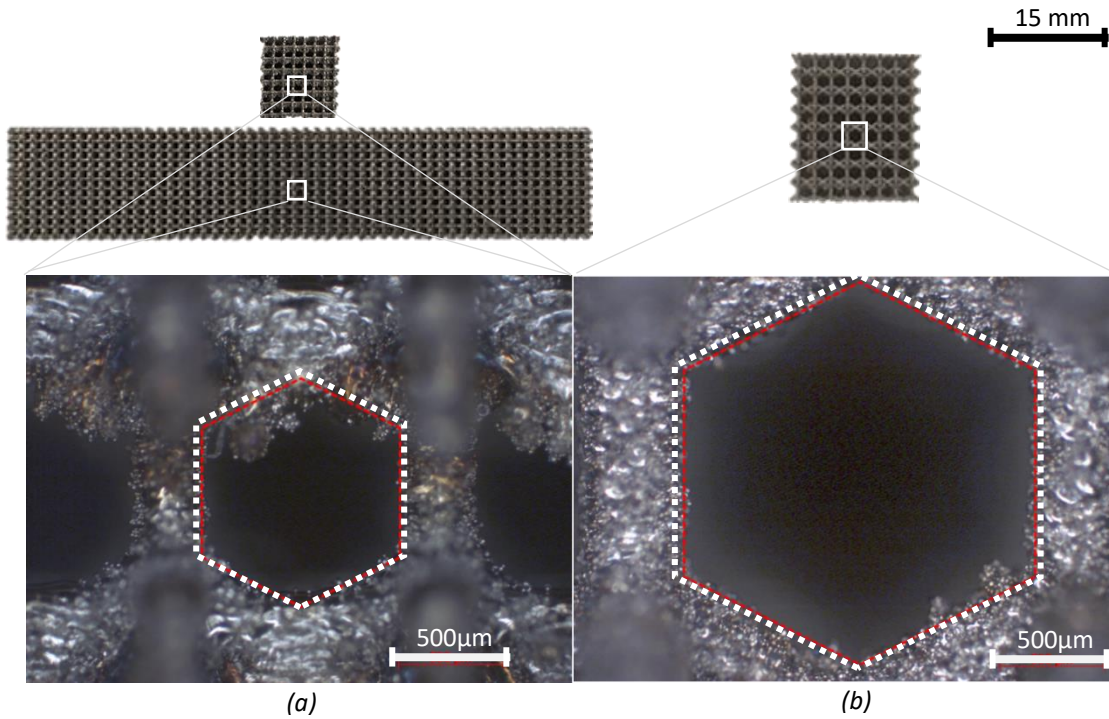


Figure 6: Optical micrographs of the unit cells of: a) the fine lattice samples and b) the coarse lattice samples. The target geometry is marked to demonstrate the extent of loose powder adhesion in each case.

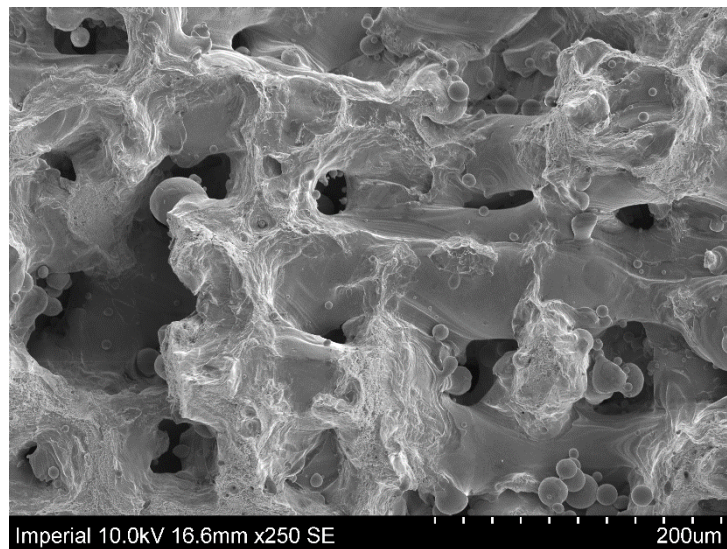


Figure 7: SEM scan of the fracture surface of a fully solid AM sample showing the porosity and spherical unfused powder particles.

3.2 Quasi-static compression and 3-point bending

Figure 8 and Figure 9 shows the stress-strain trace of the interrupted compression test of the coarse and fine lattice structure samples, showing the unloading curve. The loading region is curvilinear and fails to provide a consistent effective modulus measurement. The unloading curve displays a consistent gradient and

thus a consistent effective modulus value. The effective modulus of the coarse and fine lattice structures was

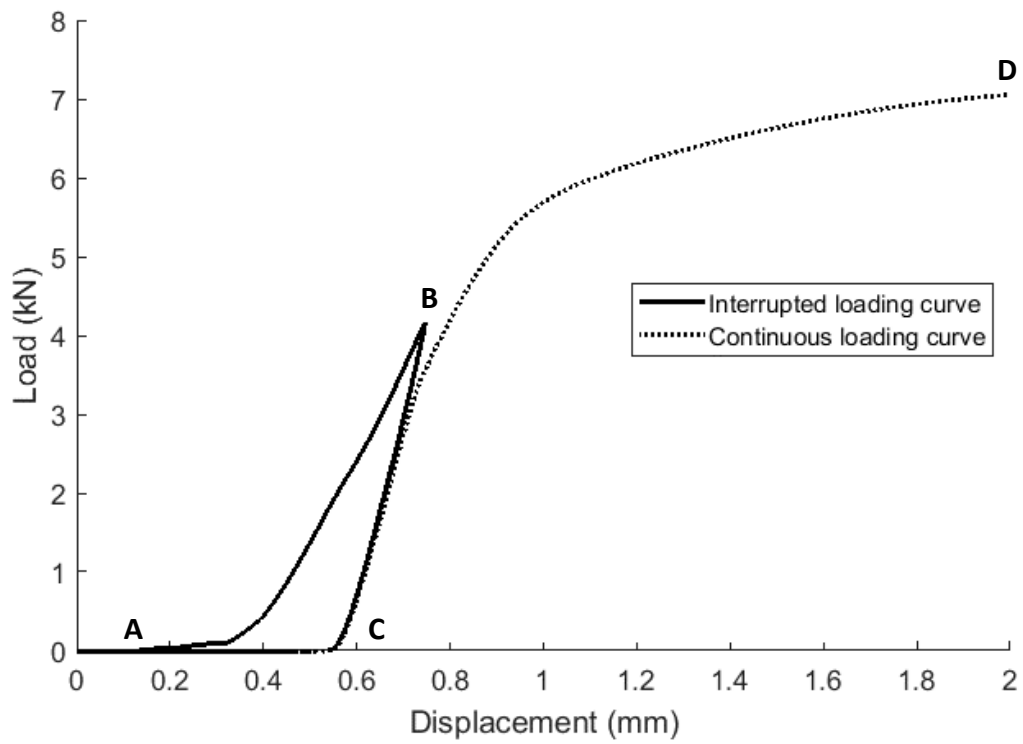


Figure 8: The interrupted load-displacement plot of the quasi-static compression test of the coarse lattice structure sample, showing the loading (curve A-B), the unloading (curve B-C) and the continuous loading curve (curve C-D).

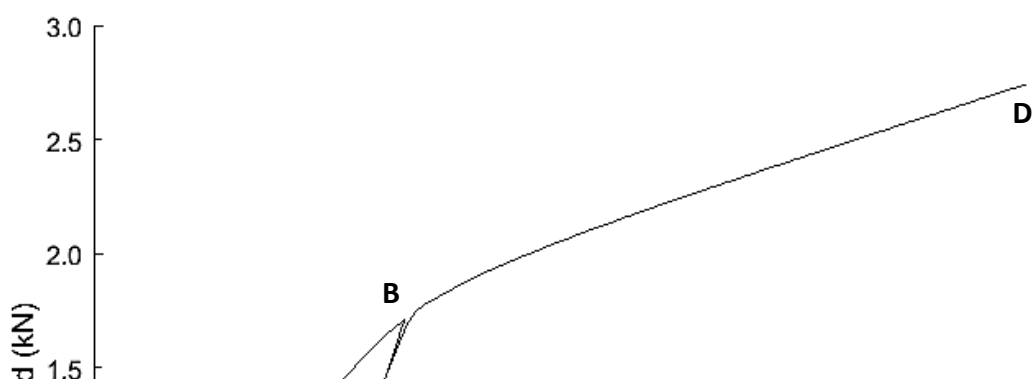


Figure 9: The interrupted load-displacement plot of the quasi-static compression test of the fine lattice structure sample, showing the loading (curve A-B), the unloading (curve B-C) and the continuous loading curve (curve C-D).

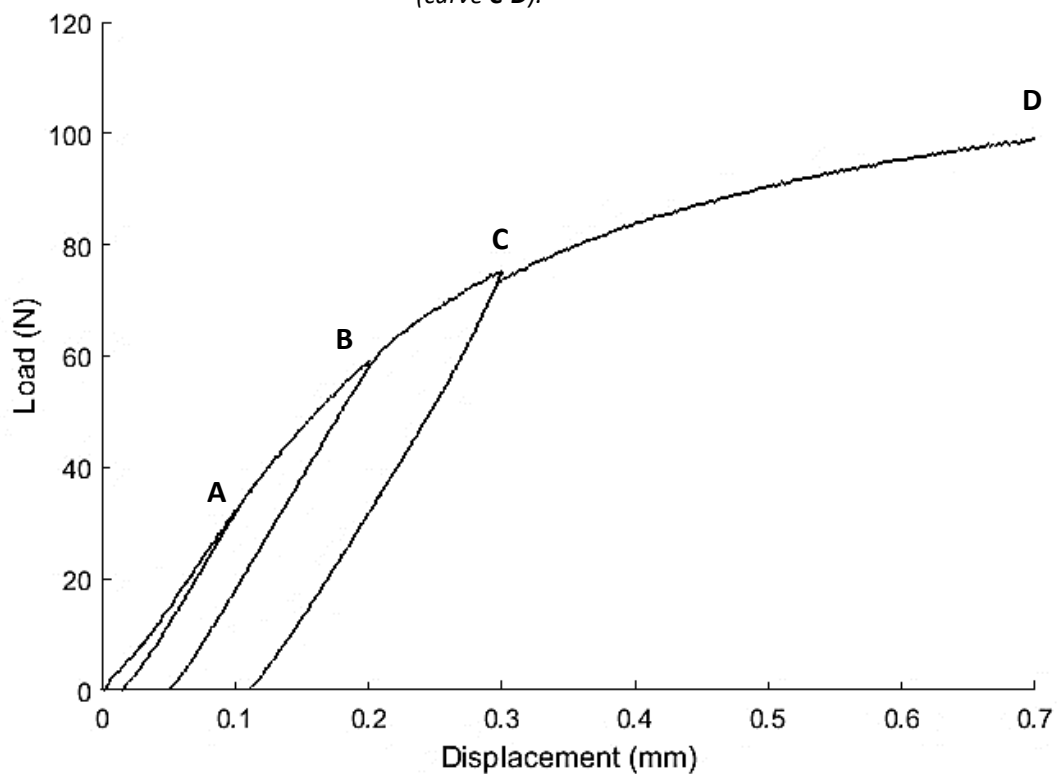


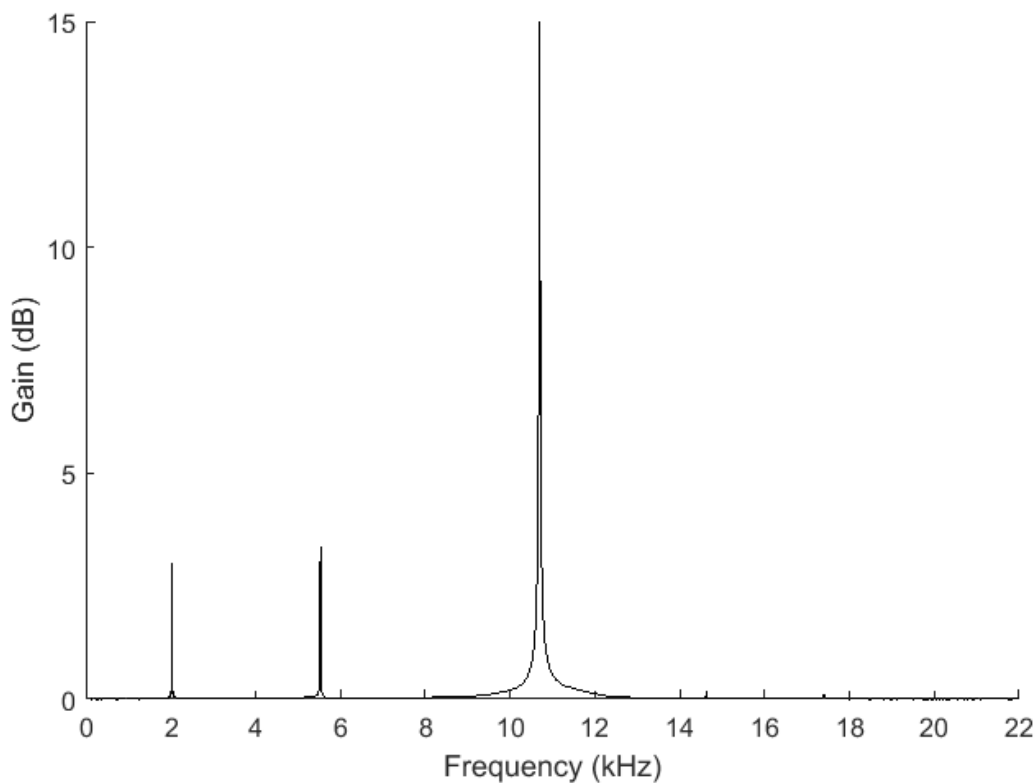
Figure 10: Load-displacement plot of the three-point bend test carried out on the AM fine lattice samples showing the interrupted loading pattern used to measure the flexural elastic stiffness of the structure with three unloading cycles A, B and C.

The load-displacement trace in Figure 10 shows the typical response expected under flexure. The interrupted elastic measuring method was again used to measure the effective modulus of the structure in flexure, which was found to be 5.6 ± 1.4 GPa. This is in close agreement with the effective modulus value measured using the fine lattice uniaxial compression tests, suggesting the structure is isotropic.

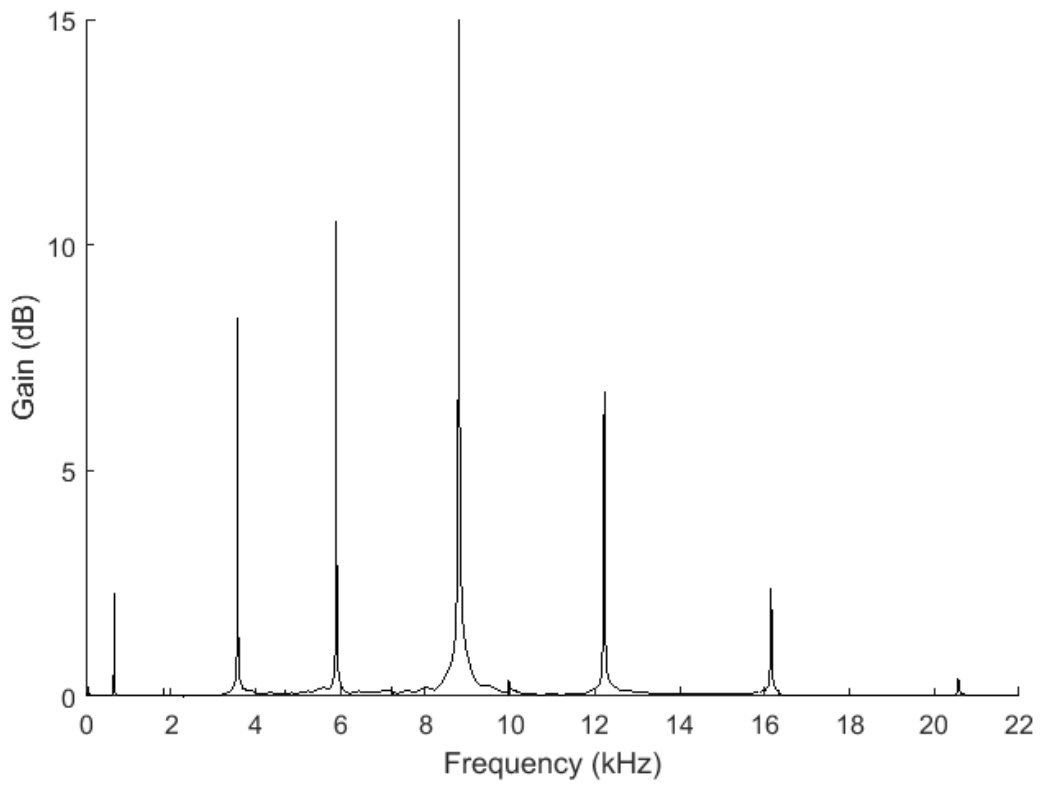
3.3 AR testing

Testing was conducted on solid 316L stainless steel sample, solid aluminium sample, fully solid AM sample and lattice AM sample (which had a fine lattice) with results shown in Figure 11. The measured fundamental resonant frequencies are summarised in

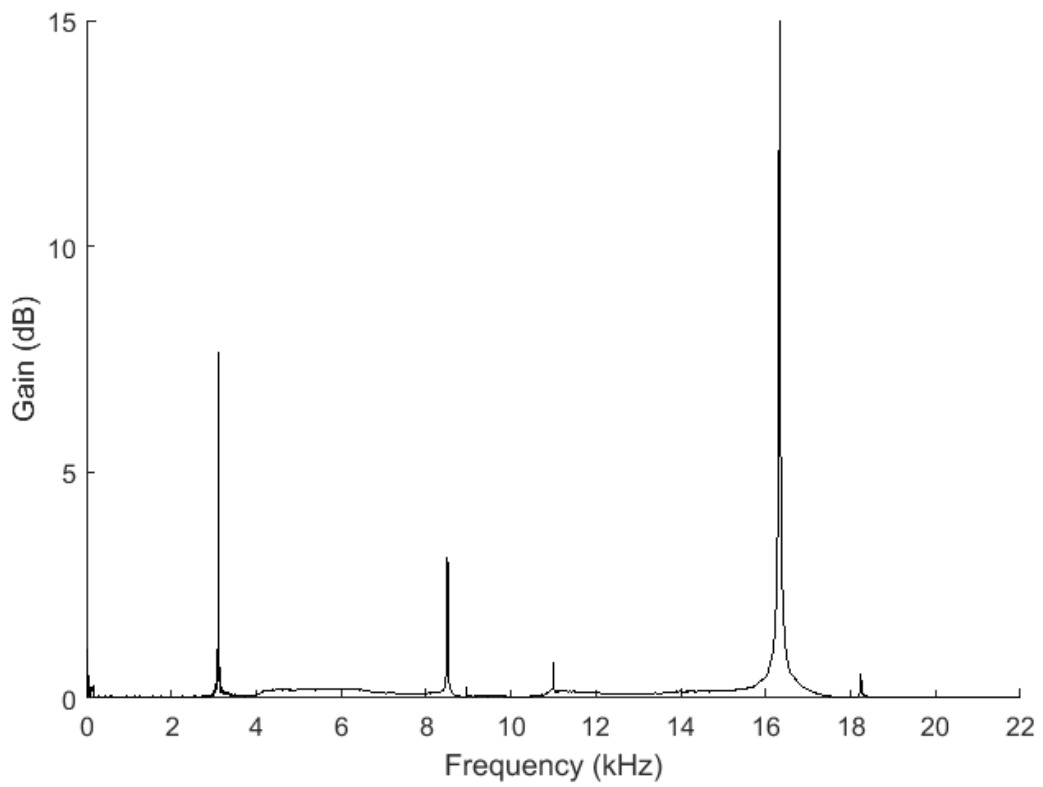
Table 5, along with the dimensional and mass measurements of the samples as well as the evaluated elastic modulus measurements. The effective modulus measurements of the fine lattice structures obtained are higher than expected in contrast to the measurements taken from the FE quasi-static compression and AR test. However, the values remain consistent throughout the sample set of ten samples, indicating consistency in the build quality. The fully solid AM samples presented slightly reduced elastic moduli values than those of the wrought 316L stainless steel samples. This can be accounted for by considering the porosity present in the AM samples [4]. This reduces the overall performance and structural parameters when compared to the wrought constituent material.



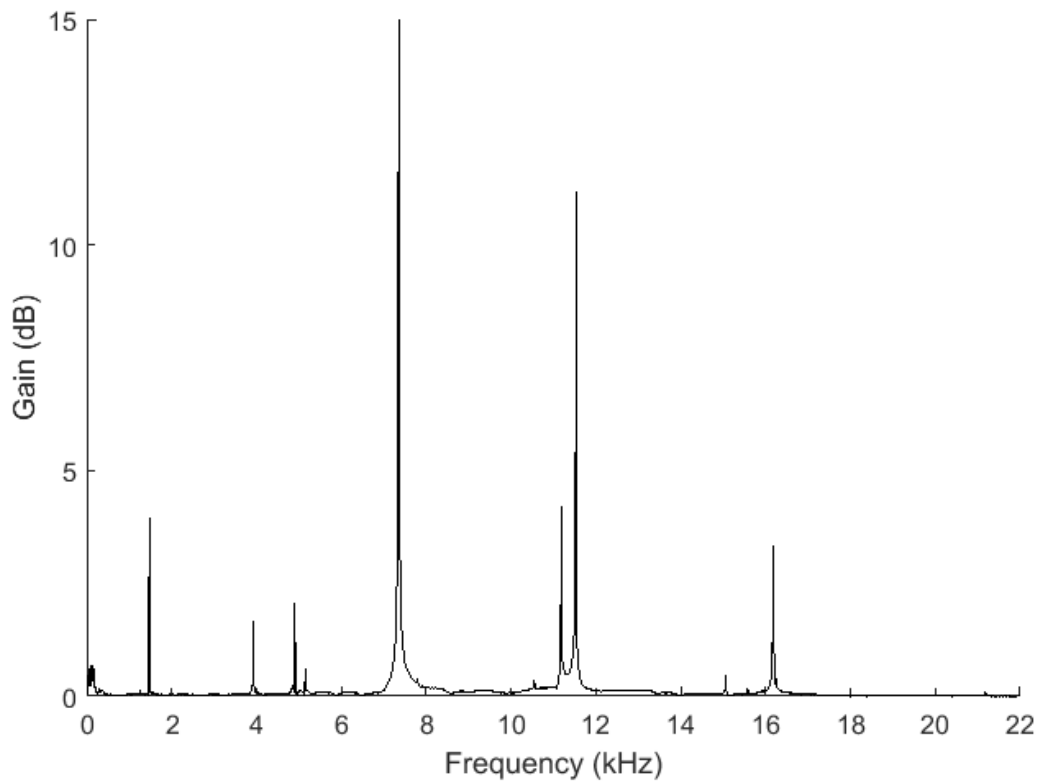
(a) 6082-T6 Aluminium calibration sample of size 99.9 x 14.7 x 3.8 mm and mass



(b) Wrought 316L stainless steel sample if size 149.9 x 25.1 x 3.0 mm and mass 86.2 g.



(c) AM solid 316L stainless steel sample of size 77.6 x 15.6 x 4.1 mm and mass 36.6 g.



(d) AM lattice 316L stainless steel sample of size 77.2 x 15.5 x 3.9 mm and mass 7.4 g.

Figure 11: The FFT frequency spectrums showing the resonant frequencies of: a) the 6082-T6 aluminium calibration sample, b) the wrought 316L stainless steel sample, c) the AM solid 316L stainless steel sample and d) the AM lattice 316L stainless steel sample (with a fine lattice).

Table 5: Specifications of the test specimens with their respective fundamental resonant frequency and the calculated effective modulus.

Sample	Length, L (mm)	Width, W (mm)	Thickness, T (mm)	Mass, m (g)	Fundamental, ω_n (Hz)	Effective modulus, E_{eff} (GPa)
6082 – T6 Aluminium	99.9	14.7	3.8	14.6 ± 0.1	2,033 ± 1	71.3
Wrought 316L Stainless Steel	149.9	25.1	3.0	86.2 ± 0.1	653 ± 2	194.5
Solid AM 316L Stainless Steel	77.6	15.6	4.1	36.6 ± 0.1	3,079 ± 5	142.7
Lattice 316L Stainless Steel (fine lattice)	77.2	15.5	3.9	7.4 ± 0.05	1,484 ± 5	7.6

The additional overtones measured during the resonance tests are used to recalculate the effective elastic modulus, allowing for multiple measurements to be taken from a single test. Table 6 and Table 7 show

the detected overtones and the solutions of expression 2.3 the resonant frequencies of the calibration samples as well as the lattice structure samples. The values are consistent throughout the various overtones, providing independent validation of the modulus measurement.

Table 6: The detected overtones measured during the AR test for the calibration samples and the lattice structure samples.

Sample	Resonant Frequency, ω_n (Hz)				
	Fundamental	1 st Harmonic	2 nd Harmonic	3 rd Harmonic	4 th Harmonic
<i>6082 – T6 Aluminium</i>	2,033 ± 1	5,534 ± 1	10,700 ± 2	17,402 ± 2	-†
<i>Wrought 316L Stainless Steel</i>	653 ± 2	1,796 ± 3	3,516 ± 5	5,800 ± 6	8,638 ± 7
<i>Solid AM 316L Stainless Steel</i>	3,079 ± 5	8,481 ± 12	16,353 ± 18	-†	-†
<i>Lattice 316L Stainless Steel</i>	1,484 ± 5	3,938 ± 11	7,387 ± 22	11,580 ± 39	16,270 ± 50

† In these cases, the frequencies are expected to be higher than that detectable by the apparatus (with a 22 kHz Nyquist limit) due to sampling rate of the audio processor.

Table 7: The elastic and effective modulus values obtained by evaluating expression 2.3 using the measured resonant frequency values

Sample	Effective modulus, E_{eff} (GPa)				
	Fundamental	1 st Harmonic	2 nd Harmonic	3 rd Harmonic	4 th Harmonic
<i>6082 – T6 Aluminium</i>	70.67 ± 0.01	68.92 ± 0.01	67.02 ± 0.02	64.89 ± 0.02	-
<i>Wrought 316L Stainless Steel</i>	180.01 ± 0.02	179.48 ± 0.03	178.94 ± 0.01	178.23 ± 0.01	177.13 ± 0.02
<i>Solid AM 316L Stainless Steel</i>	142.66 ± 0.20	142.47 ± 0.32	137.81 ± 0.37	-	-
<i>Lattice 316L Stainless Steel</i>	7.47 ± 0.30	6.93 ± 0.30	6.34 ± 0.40	5.70 ± 0.40	5.04 ± 0.50

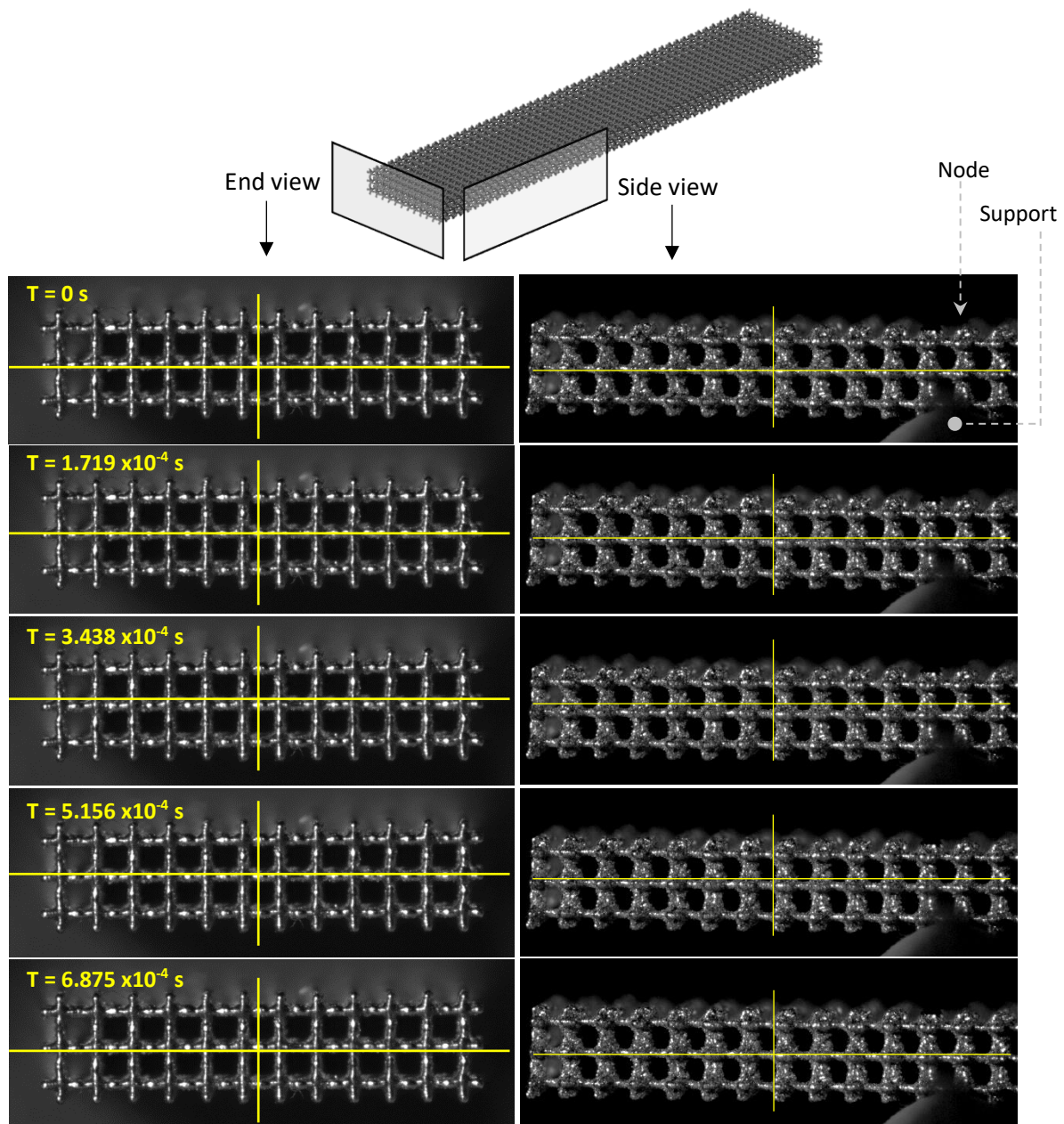


Figure 12: High-speed photography setup used to verify the vibration modes measured during the AR test. The end view ensures the torsional modes are not excited and the side view verifies the lack of movement at the antinode of the fundamental

To provide further confidence, high-speed photography, as shown in Figure 12, was used to confirm the fundamental frequency measured during the AR is indeed the resonant frequency of interest. The period of vibration after excitation was measured to be 11 frames of the high-speed footage recording at 16,000 frames per second. This equates to a fundamental frequency of $1,454.5 \pm 145$ Hz. This is similar to the value recorded in Table 6.

3.4 FE modelling

Firstly, the quasi-static compression tests of the lattice structure were modelled. This is for solid calibration samples and the lattice structure samples. Figure 13 shows the traces of the uniaxial compression of the coarse and fine lattice structure cube samples obtained experimentally and compared with the FE model. They exhibited generally good agreement and FE predicted a slightly higher elastic modulus, as well as an accurate strain for densification, as determined by the knee-point. The higher effective modulus, 2.62 GPa, predicted by the FE model is a consequence of the lack of structural defects in the model which tend to reduce the modulus in the experimental samples. The fine lattice experimental samples exhibited densification at a lower strain relative to the coarse lattice experimental samples. Densification is brought on earlier than expected, from the FE model, due to loose powder adhesion as well as the smaller sample size.

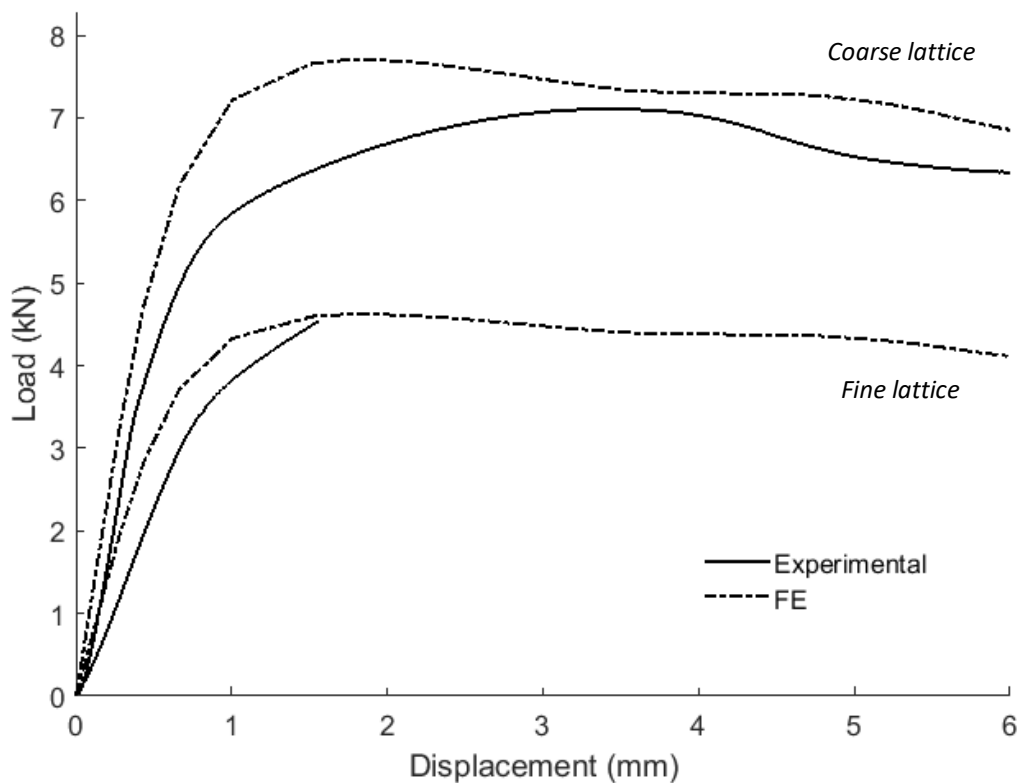


Figure 13: The load-displacement traces of the quasi-static compression of the coarse and fine lattice structures. This is both experimental and FE modelling data.

Secondly, the AR test simulations of the solid calibration samples were used to evaluate the validity of the FE model. The model was found to be notably sensitive to the number of elements used for the different test samples. Figure 14 and Figure 15 show the relationship between the number of finite elements used and the resulting resonant frequency predictions up to the fourth harmonic, for the solid aluminium calibration sample and the stainless steel lattice structure sample respectively. The experimentally measured frequencies are also included as horizontal dashed lines, with the exception of the 4th harmonic where the sampling frequency of the audio processor put the frequency above the Nyquist limit. The vibrational mode shapes for each harmonic are shown in Figure 16.

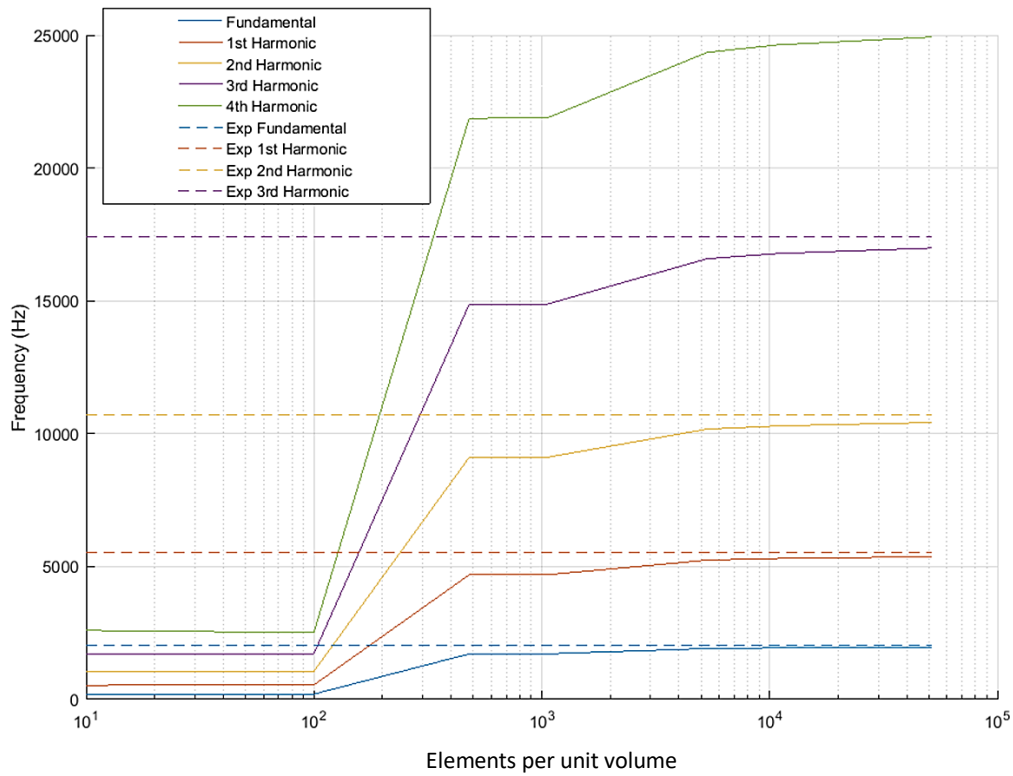


Figure 14: Sensitivity plot of the predicted resonant frequencies, of the solid aluminium calibration sample, on number of cubic FE elements used in the AR test simulation.

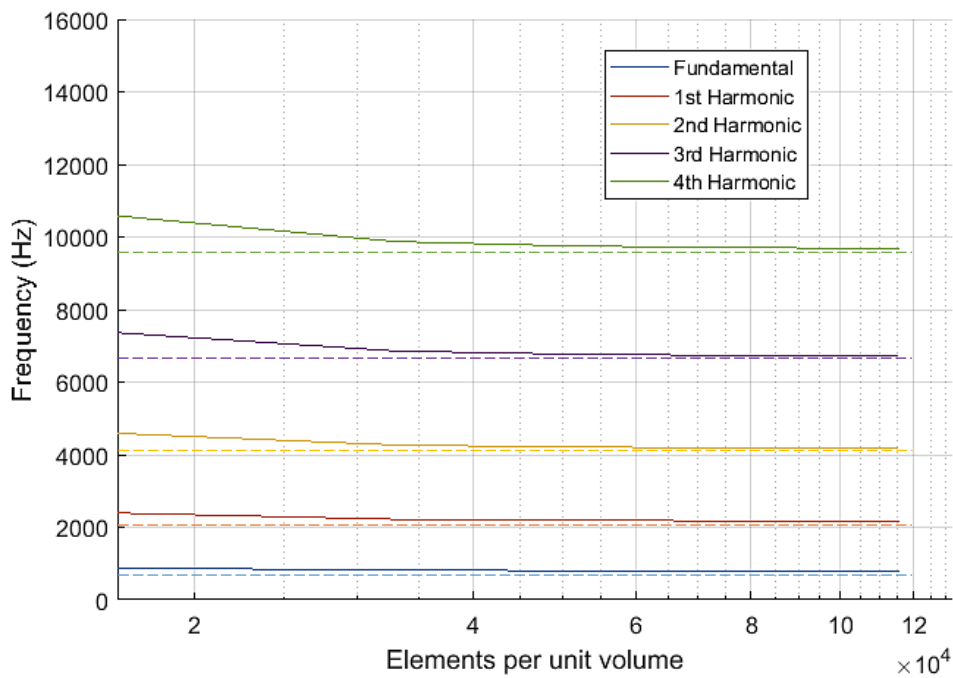


Figure 15: Sensitivity plot of the predicted resonant frequencies, of the stainless steel lattice structure sample, on number of beam FE elements used in the AR test simulation.

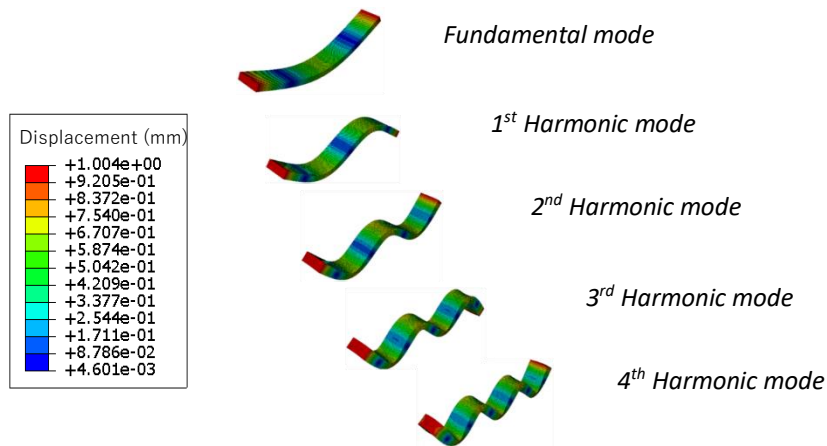


Figure 16: The vibrational modes of each resonant frequency visualised using the FE model. The colour scale indicates displacement in order to emphasise the nodes and anti-nodes of each mode. The lattice structure vibration modes also take these exact mode shapes.

For the solid aluminium calibration sample (Figure 14), the predicted frequencies are underestimated when using a low number of elements. The frequencies then tend towards the experimentally verified values as the number of elements increases. A plateau region is then reached at around 500 elements. This may be problematic as is the case for the 3rd harmonic where the aforementioned plateau resides very close to an undesired out-of-plane resonant frequency at around 14,630 Hz. This may lead to the incorrect identification of the required modes of vibration for the ensuing calculations, leading to an incorrect prediction of the value of the elastic modulus. Note that a relatively larger number of elements are required to predict accurately the higher order harmonic in comparison to the fundamental. A high number of elements was then used for the lattice structural samples tests for this reason.

For the lattice structure acoustic test simulation, the predicted frequencies are initially overestimated when using the minimum amount of elements (one beam element per lattice beam). The results then tend towards the values calculated using the design nominal relative density and equation 2.3, along with the effective modulus measurement obtained from the FE quasi-static compression tests. The overall error however is minimal when compared to the solid sample FE AR simulation partly due to the lower limit of possible elements needed to accurately represent the lattice structure.

The predicted resonant frequencies and effective modulus values of the lattice structure samples are shown in Table 8 and Table 9 respectively, as well as the predicted resonant frequencies of the calibration solid samples. The values for the lattice structure samples are lower than those obtained from the experimental tests. This is due to the lack of loose powder adhesion in the model, providing a metric for the extent of loose powder adhesion in the AM sample. The values of the solid calibration samples are very similar to those obtained experimentally.

Table 8: The predicted resonant fundamental frequencies of the test samples obtained from the FE AR test simulation.

Sample	Resonant Frequency, ω_n (Hz)				
	Fundamental	1 st Harmonic	2 nd Harmonic	3 rd Harmonic	4 th Harmonic
6082 – T6 Aluminium	2,015	5,512	10,690	17,414	25,545
Wrought 316L Stainless Steel	653	1,803	3,536	5,839	8,697
Solid AM 316L Stainless Steel	3,045	8,271	15,864	25,492	36,811
Lattice 316L Stainless Steel	798	2,174	4,180	6,723	9,686

Table 9: The effective modulus values calculated using eq. [2.3] and the resonant frequencies predicted by the FE model shown in Table 8.

Sample	Effective Modulus, E_{eff} (GPa)				
	Fundamental	1 st Harmonic	2 nd Harmonic	3 rd Harmonic	4 th Harmonic
6082 – T6 Aluminium	69.3	68.3	66.8	64.9	62.6
Wrought 316L Stainless Steel	172.9	173.5	173.6	173.2	172.2
Solid AM 316L Stainless Steel	139.6	135.6	129.7	122.6	114.6
Lattice 316L Stainless Steel	1.3	1.3	1.3	1.2	1.1

4 DISCUSSION

4.1 FE and AR comparison of modulus of elasticity values

Table 10 compares the FE and AR modulus of elasticity values with those stated in the literature. The table shows good agreement of the values and provides a measure of validation to the FE and AR techniques used in this study.

Table 10: FE and AR comparison of modulus of elasticity values

Modulus of Elasticity (GPa)	

Source	6082 – T6 Aluminium [23]	Wrought 316L Stainless Steel [24]
<i>Literature</i>	70	200
<i>AR</i>	71	180
<i>FE</i>	69	173

4.2 Effective modulus results comparison

Table 11 compiles the effective modulus measurements of the lattice structure samples obtained from the quasi-static compression tests, three-point bend tests, AR tests and the FE models. The values show fair agreement between the quasi-static compression results and the FE compression model for the coarse lattice with the FE model predicting a slightly higher elastic modulus. The AR, three-point bend and the quasi-static compression results for the fine lattice are significantly higher than those predicted by the FE AR and quasi-static compression simulations.

Table 11: The collated effective modulus values of the lattice structure samples obtained from the various tests and FE models.

Source	Lattice Size	Effective Modulus, E_{eff} (GPa)
Quasi-static compression test	Coarse	1.6 ± 0.3
Quasi-static compression test	Fine	8.6 ± 1.5
3-point bend test	Fine	5.6 ± 1.4
AR test	Fine	7.5 ± 0.5
FE simulation of the Quasi-static compression test	Coarse and fine	2.6
FE simulation of the AR test	Coarse and fine	1.3

Loose powder adhesion, as shown in Figure 6, leads to a larger relative density than expected. This is due to the laser parameters used by the AM machine as well as the particle size of the raw powder used. As the size of the cells decreases, the laser parameters need to be adjusted in order to alter the energy density deposited into the component to produce the optimum conditions to attenuate the loose powder adhesion effect. Additionally, as the size of the cells approaches the size of the powder particles used and the resolution of the AM machine, it is more difficult to reproduce the desired geometry with a tendency to worsen the loose powder adhesion effect. Furthermore, as the loose powder adhesion phenomenon is surface dependant, an increase in the surface area-to-volume ratio as the cell sizes decrease also contributes to the prominence of this

effect. It is observed as well that overhung surfaces (surfaces without direct perpendicular support underneath from the previous sintered layer) tend to accumulate more loose powder than surfaces oriented differently relative to the build direction. This tendency can be seen in Figure 6. The FE models can be assumed to be free of structural defects and loose powder adhesion.

An increase in the relative density, in this case due to loose powder adhesion, is generally expected to increase the effective modulus of the lattice structures according to Ashby et al. [18]. This effect is observed here where the fine lattice samples demonstrated an increased effective modulus across the various testing methods used. In comparison, the coarse lattice samples with measured relative density values close to the nominal design values, displayed effective modulus values very close to the analytical and FE values. It is important to note as well that the FE model overestimates the effective modulus compared to the coarse lattice AM sample results due the lack of structural defects, such as porosity and malformed struts, in the FE model [4]. The defects tend to decrease the effective modulus as well as the yield strength of the structure.

The similar effective modulus values obtained from the 3-point bend tests carried out on fine lattice samples suggest that the lattice structure is isotropic – the effective modulus in flexure and longitudinal loading is similar. This would then be expected to affect the AR results as the vibrational modes of interest in this study occur in flexure. Furthermore, the inference that this lattice structure does have a homogenous elastic response implies the suitability of expressions 2.1 and 2.3, as well as the ASTM E1803 test standard, for use with this lattice structure design as both methods assume a homogenous material sample.

In AR testing, the loose powder greatly alters the dynamic response of the structure. It can be inferred from equation 2.1 that an increase in the mass of the structure leads to a decrease in the resonant frequencies, which leads to a decrease in the calculated modulus from equation 2.3. In contradiction, in equation 2.3 an increase in mass leads to an increase in the calculated modulus. As the modulus calculated from equation 2.3 is more sensitive to change in the resonant frequency than the structural mass, an increase in mass is expected to lead to a lower stiffness measurement overall.

This however is not the case with the experimental results of the AR testing in this study, where the measured effective modulus value of the fine lattice AR samples are significantly higher than expected. This can be explained by considering the assumption that the structure is homogenous: The honeycomb structure used is thought to have homogenous in-plane properties as shown by Ashby et al. [9]. The loose powder adhesion effect, being irregular in nature and favouring overhung surfaces, is expected to introduce inhomogeneity to the structure. This would lead to an overall decrease in the effective modulus of the structure when measured using AR as explained previously. This is not the case in actuality, suggesting that the loose powder adhesion effect does lead increased structural stiffness as the added mass does contribute to load-bearing and is not simply loosely attached as dead weight.

The result predicted by the FE AR model is more in line with those predicted by the uniaxial coarse lattice compression tests and FE model, as the AR model does not have any loose powder adhesion nor structural defects and so represents the ideal geometry. The agreement in results suggests that the model has a high degree of homogeneity as expected from the ideal geometry and so equations 2.1 and 2.3 can be used to calculate the effective modulus.

4.3 Resonance test extension

The modulus values obtained by evaluating Equation 2.3 for each overtone match with those obtained using the fundamental frequency and remain fairly consistent between each overtone. This suggests the method's suitability for validating the elastic modulus measurements obtained using the AR test. The flexibility of the test is also extended as the need for carefully supporting the sample to isolate the fundamental is reduced, allowing for in-situ testing.

A trend is observed where the higher overtones show a slight decrease in the modulus measurement. This implies strain-rate dependence as the higher overtones operate at higher frequencies, hence higher strain rates. This may be used to obtain information on the strain rate dependency from the AR test as well.

This method strongly relies on the correct identification of the order and mode of the natural frequency. It is important therefore to predict the frequencies of the desired overtones as well as the undesired vibrational modes for proper selection of the measured frequencies used in the calculation of the dynamic moduli. This must also take the support conditions of the component into account for in-situ testing.

5 CONCLUSIONS

The main research findings can be summarized as follows:

- There is a dependence of the relative density on the cell size when maintaining the same laser parameters and feed powder particle size. These factors need to be optimized when varying the cell size to achieve more faithful recreation of the desired geometry.
- Both the quasi-static compression lattice structure samples and the AR test samples exhibited higher relative densities than design value due to the loose powder adhesion effect, with the coarse lattice compression samples deviating by 10.9% and the fine lattice AR samples deviating by 62.2%.
- The AM solid samples exhibit a lower relative density than expected due to the internal porosity present in the samples caused by a lack of fusion of the raw powder material.
- The effective modulus measurements obtained from the compression tests and the AR tests of the fine lattice were higher than those obtained from the coarse lattice tests as well as the FE simulation of quasi-static compression and the AR test.
- The effective modulus value predicted by the compression test FE simulation was slightly higher than that of the experimental test of the coarse lattice due to the absence of microscopic structural defects in the model, which exist to some extent in the AM samples.
- The effective modulus values obtained from the 3-point bend tests of the fine lattice were similar to those obtained from the uniaxial compression tests, suggesting that the structure is homogenous and isotropic despite the loose powder adhesion effect.
- The AR can be used to measure the modulus of AM lattice samples with high degree of loose powder adhesion, and may be used directly to provide a metric of loose powder adhesion and other related structural characteristics by means of comparison with the expected analytical values. Future testing of other AM lattice structures using AR is recommended.

- The resonance test extension suggested is capable of obtaining accurate modulus measurements from the higher overtones detected during the test, allowing for greater flexibility as well as added insight into the strain-rate dependency of the material/lattice structure.

ACKNOWLEDGEMENTS

The strong support from the Aviation Industry Corporation of China (AVIC) Manufacturing Technology Institute (MTI) for this funded research is much appreciated. The research was performed at the AVIC Centre for Structural Design and Manufacture at Imperial College London

REFERENCES

- [1] Petrovic, Vojislav, et al. "Additive layered manufacturing: sectors of industrial application shown through case studies." *International Journal of Production Research* 49.4 (2011): 1061-1079.
- [2] Fleck, N. A., V. S. Deshpande, and M. F. Ashby. "Micro-architected materials: past, present and future." *Proceedings of the Royal Society of London: Mathematical, Physical and Engineering Sciences*. Vol. 466. No. 2121. The Royal Society, (2010).
- [3] Gibson, Lorna J., and Michael F. Ashby. "Cellular solids: structure and properties." Cambridge university press, (1997). PP: 20-156
- [4] Park, Sang-In, et al. "Effective mechanical properties of lattice material fabricated by material extrusion additive manufacturing." *Additive Manufacturing* 1 (2014): 12-23.
- [5] Xiao, Z., Yang, Y., Xiao, R., Bai, Y., Song, C., and Wang, D., "Evaluation of topology-optimized lattice structures manufactured via selective laser melting." *Materials & Design* 143 (2018): 27-37.
- [6] Niu J., Choo H., Sun W., and Mok S., "Analytical Solution and Experimental Study of Effective Young's Modulus of Selective Laser Melting-Fabricated Lattice Structure With Triangular Unit Cells." *ASME. J. Manuf. Sci. Eng.* 140.9 (2018); 1-13.
- [7] du Plessis, A., Yadroitsava, I., Yadroitsev, I., le Roux, S.G. and Blaine, D.C., "Numerical comparison of lattice unit cell designs for medical implants by additive manufacturing." *Virtual and Physical Prototyping*, 13.4 (2018) 266-281.
- [8] Shamvedi, D., McCarthy, O.J., O'Donoghue, E., Danilenkoff, C., O'Leary, P. and Raghavendra, R. "3D Metal printed heat sinks with longitudinally varying lattice structure sizes using direct metal laser sintering." *Virtual and Physical Prototyping* 13.4 (2018) 301-310.
- [9] Sing, Swee L., Florencia, Edith W., Yeong, and Wai Y., "Selective laser melting of lattice structures: A statistical approach to manufacturability and mechanical behaviour." *Robotics and Computer-Integrated Manufacturing* 49 (2018): 170-180.
- [10] Sing, S., Yeong, W., Wiria, F., and Tay, B. "Characterization of Titanium Lattice Structures Fabricated by Selective Laser Melting Using an Adapted Compressive Test Method." *Experimental Mechanics*, 56.5 (2016), 735-748.
- [11] Fatemi, S. A., Ashany, J.Z., A., Aghchai, A.J., and Abolghasemi, A. "Experimental investigation of process parameters on layer thickness and density in direct metal laser sintering: a response surface methodology approach." *Virtual and Physical Prototyping*. 12.2 (2017) 133-140.

- [12] Bland, Stewart, and Nesma T. Aboulkhair. "Reducing porosity in additive manufacturing." *Metal Powder Report* 70.2 (2015): 79-81.
- [13] Gong, Haijun, et al. "Analysis of defect generation in Ti-6Al-4V parts made using powder bed fusion additive manufacturing processes." *Additive Manufacturing* 1 (2014): 87-98.
- [14] ASTM E 1876-99, Standard test method for dynamic Young's modulus, shear modulus, and Poisson's ratio by impulse excitation of vibration. In: *Annual book of ASTM standards, ASTM International*, vol. 03.01; (1999).
- [15] M-Lab Cusing R Datasheet. (2017). 3rd ed. Lichtenfels: Concept Laser, pp.1-2. Available at: https://www.concept-laser.de/fileadmin/Neue_Produnkte/1610_Mlab_cusing_R_EN.pdf [Accessed 22 Jun. 2017].
- [16] Ghose, S., Babu, S., Van Arkel, R.J., Nai, K., Hooper, P. and Jeffers, J.R.T., "The influence of laser parameters and scanning strategies on the mechanical properties of a stochastic porous material." *Materials & Design* 131 (2017): 498-508
- [17] Ghose, S., Babu, S., Nai, K., Hooper, P. and Jeffers, J.R.T., "The influence of laser parameters, scanning strategies and material on the fatigue strength of a stochastic porous structure." *Additive Manufacturing* 22 (2018): 290-301
- [18] Ashby, Michael F., Evans, A.G., Fleck, N.A., Gibson, L.J., Hutchinson, J.W. and Wadley, H.N.G., "Metal foams: a design guide." *Butterworth-Heinemann*, (2000). PP.63-67
- [19] ASTM D 1621-16, Standard test method for Compressive Properties of Rigid Cellular Plastics. In: *Annual book of ASTM standards, ASTM International*, vol. 08.01; (2016).
- [20] ASTM D790—17 Standard Test Methods for Flexural Properties of Unreinforced and Reinforced Plastics and Electrical Insulating Materials. In: *Annual book of ASTM standards, ASTM International*, vol. 08.01; (2017).
- [21] Hibbitt, Karlsson, Sorensen. ABAQUS/Standard user's manual. *Hibbitt, Karlsson & Sorensen*; (2014).
- [22] Galarraga, Haize, et al. "Effects of the microstructure and porosity on properties of Ti-6Al-4V ELI alloy fabricated by electron beam melting (EBM)." *Additive Manufacturing* 10 (2016): 47-57.
- [23] Aalco Metals Ltd "Aluminium Alloy 6082 - T6~T651 Plate." *Wednesbury* (2016): 1-2.
- [24] Penn Stainless Products, Inc. "Alloy 316/316L Specifications: UNS S31600 / S31603" *Pennsylvania* (2018): 1-2.